Synthesis and Biophysical Properties of Arabinonucleic Acids (ANA): Circular Dichroic Spectra, Melting Temperatures, and Ribonuclease H Susceptibility of ANA·RNA Hybrid Duplexes†

Anne M. Noronha,‡ Christopher J. Wilds,‡,§ Chun-Nam Lok,|| Katya Viazovkina,‡ Dominique Arion,|| Michael A. Parniak,|| and Masad J. Damha*,‡

Department of Chemistry, McGill University, Montreal, Quebec, Canada H3A 2K6, and McGill AIDS Centre and Faculty of Medicine, McGill University, Montreal, Quebec, Canada H3T 1E2

Received February 7, 2000; Revised Manuscript Received April 10, 2000

ABSTRACT: Arabinonucleic acid (ANA), the 2′-epimer of RNA, was synthesized from arabinonucleoside building blocks by conventional solid-phase phosphoramidite synthesis. In addition, the biochemical and physicochemical properties of ANA strands of mixed base composition were evaluated for the first time. ANA exhibit certain characteristics desirable for use as antisense agents. They form duplexes with complementary RNA, direct RNase H degradation of target RNA molecules, and display resistance to 3′-exonucleases. Since RNA does not elicit RNase H activity, our findings establish that the stereochemistry at C2′ (ANA versus RNA) is a key determinant in the activation of the enzyme RNase H. Inversion of stereochemistry at C2′ is most likely accompanied by a conformational change in the furanose sugar pucker from C3′-endo (RNA) to C2′-endo ("DNA-like") pucker (ANA) [Noronha and Damha (1998) *Nucleic Acids Res. 26*, 2665−2671; Venkateswarlu and Ferguson (1999) *J. Am. Chem. Soc. 121*, 5609−5610]. This produces ANA/RNA hybrids whose CD spectra (i.e., helical conformation) are more similar to the native DNA/RNA substrates than to those of the pure RNA/RNA duplex. These features, combined with the fact that ara-2′OH groups project into the major groove of the helix (where they should not interfere with RNase H binding), help to explain the RNase H activity of ANA/RNA hybrids.

The past decade has seen a tremendous growth in the use of synthetic oligonucleotide analogues in medicinal chemistry (*1*, *2*). The drug Vitravene (ISIS-2922) has recently been granted approval by the U.S. Food and Drug Administration for the treatment of cytomegalovirus (CMV) induced retinitis, and other compounds are currently in clinical trial for the treatment of cancer, inflammation, and viral infections (*1*, *3*). Recent research has yielded second-generation oligonucleotide analogues (AON)[1] that have chemical stability and resistance to nuclease degradation, yet sufficient specificity to bind to a particularly mRNA target through Watson−Crick base-pairing interactions (*3*). "Antisense therapy", as it is called, is based on this exquisite AON−mRNA interaction and the subsequent inhibition of protein synthesis caused by such AON (*4*).

Many problems related to this approach, such as large-scale production of antisense oligonucleotide analogues (AONs) (*5*) or efficient transport and delivery (*6*), are gradually being overcome through major advances in chemistry (*7*). One remaining challenge, however, is the need to develop AONs that combine specificity and high mRNA affinity while retaining the ability to activate RNase H. The latter requirement is particularly important since RNase H potentiates the biological activity of AONs by degrading the mRNA portion of the AON−mRNA duplex and releasing the AON (*8*, *9*). Although RNase H cleaves only the RNA strand of the hybrid, this action is very much dependent on the nature of the bound AON strand. For example, *Escherichia coli* RNase H1 acts upon DNA−RNA hybrids (the native substrate in vivo), but it will not degrade double-stranded RNA (*10*−*13*). Understanding the requirements for RNase H activation should therefore aid in the development of antisense drugs.

† This research was supported by Strategic Grant STR-181477 from the National Sciences and Engineering Research Council of Canada (NSERC) and by a grant from the Medical Research Council of Canada to both M.J.D. and M.A.P. C.J.W. is a recipient of NSERC postgraduate and postdoctoral scholarships. M.A.P. is an International Research Scholar of the Howard Hughes Medical Institute, and M.J.D. is the recipient of the 1999 Merck-Frosst Award for Therapeutic Research (CSC).

* To whom correspondence should be addressed at the Otto Maass Chemistry Building, 801 Sherbrooke St. W., Montreal, Quebec, Canada H3A 2K6. Tel: (514) 398-7552. Fax: (514) 398-3797. E-mail: damha@chemistry.mcgill.ca.

‡ Department of Chemistry.

§ Current address: Department of Molecular Pharmacology and Biological Chemistry, Northwestern University Medical School, Chicago, IL.

|| McGill AIDS Centre and Faculty of Medicine.

[1] Abbreviations: ANA, arabinonucleic acid; AON, antisense oligonucleotide; CD, circular dichroism; CPG, controlled pore glass; COSY, double-quantum-filtered correlated spectroscopy; DBU, 1,8-diazabicyclo-[5.4.0]undec-1-ene; ssDNA, single-stranded DNA; DMAP, 4-(dimethylamino)pyridine; DMSO, dimethyl sulfoxide; FAB, fast atom bombardment; 2′F-ANA, 2′-deoxy-2′-fluoroarabinonucleic acid; FC, flash column; MALDI-TOF, matrix-assisted laser desorption ionization time of flight; MMT, monomethoxytrityl; NBA, 4-nitrobenzyl alcohol; NMR, nuclear magnetic resonance; NPE, 4-nitrophenylethyl; RNase H, ribonuclease H; RT, reverse transcriptase; SVPDE, snake venom phosphodiesterase; TBAF, tetra-*n*-butylammonium fluoride; THF, tetrahydrofuran; TLC, thin-layer chromatography.

10.1021/bi000280v CCC: $19.00
Published on Web 05/20/2000

Chart 1

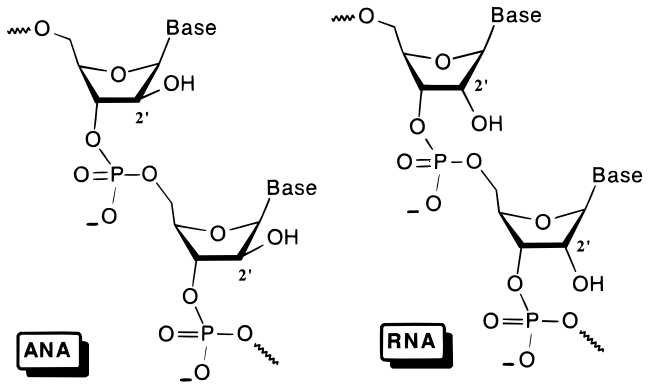

Several studies using chemically modified AON suggest that the enzyme interacts not with the hybrid's major groove but with its minor groove (*13*−*16*). Since RNA fails to activate RNase H for cleaving the target RNA after hybridization, and the ribose 2′OH (or 2′O-alkyl) groups point into the minor groove of the helix, the implication drawn is that such groups may interfere with the catalytic process of RNase H (*15*, *17*). The narrower minor groove width of the DNA−RNA hybrid relative to the pure RNA duplex likely plays a role in substrate discrimination (*13*, *18*). A third, perhaps related explanation is the flexible conformation of the hybrid as compared to the pure RNA duplex. Whereas A-form RNA duplexes are characterized by C3′-endo puckered sugars, a more complex structure characterizes the DNA−RNA hybrids: an A-type C3′-endo puckering for riboses and a dynamic puckering (multiple conformers in exchange) or O4′-endo puckering for deoxyriboses (*18*, *19*). These structural features are thought to permit specific (optimal) interactions between RNase H and the hybrid polynucleotide strands (*15*, *18*).

In an extension of our research on the synthesis and properties of ANA strands (*20*−*22*), we now report a comprehensive study covering the synthesis and biophysical properties of ANA (2′OH) (Chart 1). Specifically, we describe duplex-forming properties of RNA and DNA with a range of ANA (2′OH) sequences containing six nucleobases (adenine, uracil, thymine, cytosine, guanine, and hypoxanthine). We also examine the effect of base mismatches on ANA−RNA duplex stability. Other goals in the present study were to further evaluate the behavior of ANA with respect to its stability to nucleases and its ability to form hybrids with RNA that are susceptible to the enzyme RNase H. Indeed, we show that ANA, unlike the 2′-epimeric RNA, directs RNase H degradation of target RNA. This establishes that the configuration at the 2′-position of the antisense strand determines the ability to activate RNase H. A preliminary account of some of these results has appeared (*23*).

MATERIALS AND METHODS

Materials. Dichloromethane, pyridine, collidine, and *N*,*N*-dimethylformamide were dried over calcium hydride. Triethylamine tris(hydrofluoride) and tetra-*n*-butylammonium fluoride (1.0 M TBAF in THF) were used as obtained (Aldrich). Thin-layer chromatography (TLC) was carried out on analytical Merck silica plates (Kieselgel 60 F-254; 0.2 mm thickness). Column chromatography was performed with silica gel (40−63 μm). Compounds on TLC were visualized by UV shadowing or by dipping the plate in Mohr's solution (2.5 g of ammonium molybdate and 1 g of ceric sulfate in 10% sulfuric acid, w/v) followed by heating.

Spectra. NMR spectra were run in $CDCl_3$ or DMSO-d_6 on a Varian XL500 instrument; ^{1}H and ^{31}P chemical shifts (δ, ppm) are relative to tetramethylsilane and 85% H_3PO_4 (external reference), respectively. ^{1}H NMR assignments were facilitated by recording homonuclear correlated spectra (COSY). MALDI-TOF mass spectra were obtained on a Kratos Kompact-III instrument operated in a positive reflector or linear mode. The matrix was 20 mM ammonium citrate in acetonitrile−water (1:1, v/v) containing 6-aza-2-thiothymine (10 mg/mL). Generally, 5 μL of sample (1 mM) was pipetted into an Eppendorf tube, to which was added 5 μL of the matrix. The final solution was shaken briefly, and 1−3 μL was applied to a stainless steel sample slide and air-dried prior to analysis. FAB mass spectra were obtained on a Kratos MS25RFA spectrometer using 2-nitrobenzyl alcohol (NBA) as the matrix.

Circular dichroism spectra were obtained on a Jasco J-710 spectropolarimeter equipped with a NESLAB RTE-111 circulating bath. Samples were allowed to equilibrate for 5−10 min at the appropriate temperatures (buffer: 140 mM K^+, 1 mM Mg^{2+}, and 5 mM Na_2HPO_4, pH 7.2). Each spectrum was an average of five scans and was collected at a rate of 100 nm/min with a bandwidth of 1 nm and sampling wavelength of 0.2 nm. The CD spectra were recorded from 350 to 200 nm at 5 °C and normalized by subtraction of the background scan with buffer. The molar ellipticity was calculated from the equation $[\theta] = \theta/Cl$, where θ is the relative ellipticity (millidegrees), C is the molar concentration of oligonucleotides (moles per liter), and l is the path length of the cell (centimeters). The data were processed on a PC computer using Windows-based software supplied by the manufacturer (JASCO, Inc.).

UV Thermal Denaturation Studies. UV thermal denaturation data were obtained on a Varian Cary 1 UV−vis spectrophotometer equipped with a Peltier temperature controller. Molar extinction coefficients for oligoarabinonucleotide strands were calculated using the nearest-neighbor approximation and were assumed to be the same as those of RNA strands (*24*). Samples were heated to 80−90 °C for 15 min, then cooled slowly to room temperature, and stored at 4 °C overnight before measurements. Prior to the thermal run, samples were degassed by placing them in a Savant lyophilizer (2 min). Absorbance values were recorded after equilibration as the temperature was increased incrementally 0.5 °C at 1-min intervals (buffer: 140 mM K^+, 1 mM Mg^{2+}, and 5 mM Na_2HPO_4, pH 7.2). To compare relative overall changes in absorbance, normalized ΔA plots were constructed according to the method of Wilson and co-workers (*25*) by use of the formula $(A_t - A_i)/A_f$, where A_i is the initial absorbance and A_f is the final absorbance. Hyperchromicity values (% H) are reported as the percent increase in absorbance at the wavelength of interest with respect to the final absorbance. T_m values were calculated using the baseline method reported by Puglisi and Tinoco (*24*) and have generally an uncertainty of ±0.5 °C.

Arabinonucleoside Synthesis. The free (unprotected) nucleosides araC, araU, araI, and araA were obtained commercially (Sigma and Pfanstiel). For the purpose of oligonucleotide synthesis, araU, araA, and araC were converted

to the 5′-(monomethoxytrityl)-2′-*O*-acetyl-3′-*O*-(β-cyanoethyl-*N*,*N*-diisopropylphosphoramidite) derivatives (**1**−**3**) by our published procedures (*20*−*22*). AraG amidites **4a,b** were prepared by starting from guanosine as described below. Procedures for the synthesis of araI (**5**) and araT (**6**) derivatives are provided in Supporting Information.

*(A) 3′,5′-O-(1,1′,3,3′-Tetraisopropyldisiloxane-1,3-diyl)-β-*D*-guanosine (7).* To a solution of anhydrous guanosine (2.04 g, 2.83 mmol) in pyridine−DMF (5:1 v/v; 36 mL) was added dropwise 1,3-dichloro-1,1′,3,3′-tetraisopropyldisiloxane (2.6 mL, 2.83 mmol). The mixture was allowed to stir overnight and was quenched by the addition of water (35 mL). The resulting white precipitate was filtered, washed with water, and recrystallized from methanol−diethyl ether (1:1 v/v; 40 mL). Yield 2.29 g (84%). R_f (TLC, toluene−ethyl acetate−methanol, 9:9:2 v/v/v) 0.25. FAB MS, M + 1 526, M calcd 525. ^{1}H NMR (DMSO-d_6) ppm 10.6 (s, NH amide), 7.73 (s, H8), 6.5 (s, NH_2), 5.65 (d, H1′, $J_{1′,2′}$ = 1.5 Hz), 4.35 (t, H2′), 4.25 (m, H3′), 4.1(d, H4′), 3.97 (dd, H5′ and H5″), 1.00 [m, Si−CH$(CH_3)_2$ and CH_3].

*(B) O^6-[2-(4-Nitrophenyl)ethyl]-3′,5′-O-(1,1′,3,3′-tetraisopropyldisiloxane-1,3-diyl)-β-*D*-guanosine (8).* To a solution of triphenylphosphine (0.6 g, 2.8 mmol) and 2-(4-nitrophenyl)ethanol (507 mg, 3.0 mmol) in dry tetrahydrofuran (38.0 mL) was added diethyl azodicarboxylate (0.33 mL, 2.8 mmol) followed by compound **7** (1.0 g, 1.9 mmol). The mixture was allowed to stir for 2 h, concentrated under vacuum, and partitioned between aqueous sodium bicarbonate and chloroform. The organic layer was washed with brine, dried (magnesium sulfate), and evaporated to give an orange gum. Purification of the crude product by chromatography (toluene−ethyl acetate, 2:1 v/v) did not separate the triphenylphosphine oxide byproduct. Treatment with diethyl ether resulted in precipitation of a white spongy solid (mp 113−120 °C) believed to be triphenylphosphine oxide. A second column purification using a gradient (toluene−ethyl acetate, 3:1 to 1:1 v/v) yielded the title compound as a yellow foam. Yield 0.9 g (73%). R_f (TLC, toluene−EtOAc, 1:1 v/v) 0.19. R_f (TLC, CH_2Cl_2−MeOH, 9:1 v/v) 0.48. FAB MS, M + 1 675, M calcd 674. ^{1}H NMR (DMSO-d_6) ppm 8.16 (m, 2H ortho to NO_2), 7.89 (s, H8), 7.61 (d, 2H meta to NO_2), 6.46 (s, NH_2), 5.74 (d, H1′, $J_{1′,2′}$ = 1.5 Hz), 5.61 (d, hydroxyl proton at C2′), 4.65 (t, OCH_2CH$_2$), 4.36 (m, H2′ and H3′), 4.04 (m, H4′, H5′, and H5″), 3.22 (t, OCH$_2$CH_2), 1.12−0.98 [m, Si−C$H$$(CH_3)_2$ and CH_3].

*(C) O^6-[2-(4-Nitrophenyl)ethyl]-3′,5′-O-(1,1′,3,3′-tetraisopropyldisiloxane-1,3-diyl)-2′-O-[(trifluoromethyl)sulfonyl]-β-*D*-guanosine (9).* A solution of **8** (0.52 g, 0.77 mmol) and 4-(dimethylamino)pyridine (0.37 g, 3.1 mmol) in pyridine (0.6 mL, 6.9 mmol)−CH_2Cl_2 (10 mL) was cooled to 0 °C (1 h) and treated with trifluoromethanesulfonic anhydride (0.194 mL, 1.15 mmol). The mixture was allowed to stir at 0 °C for 5 min and then at room temperature for 3 h and finally partitioned between CH_2Cl_2 (10 mL) and water (10 mL). The organic layer was successively washed with 0.4 M HCl (2 × 12.5 mL), saturated $NaHCO_3$ (2 × 20 mL), and brine (2 × 20 mL) and finally dried over magnesium sulfate. Flash column (FC) chromatography (toluene−ethyl acetate, 6:1 v/v) yielded the title compound: 0.46 g (82%). Purification by FC chromatography was found to be unnecessary as it generally reduced yields (e.g., when the reaction was scaled up, FC purification provided compound **9** in only 43% yield). R_f (TLC, toluene−ethyl acetate, 4:1 v/v) 0.3. FAB MS, M + 1 807, M calcd 806. ^{1}H NMR ($CDCl_3$) ppm 8.17 (d, 2H, ortho to NO_2), 8.09 (s, H8), 7.53 (d, 2H meta to NO_2), 6.10 (s, H1′, $J_{1′2′}$ = 0 Hz), 5.56 (d, H2′), 4.93 (dd, H3′), 4.80 (t, OCH_2CH$_2$), 4.16 (m, H4′), 4.26−4.0 (m, H5′ and H5″), 3.31 (t, OCH$_2$CH_2), 1.02 [m, Si−C$H$$(CH_3)_2$ and CH_3 from 4 *i*-Pr].

*(D) O^6-[2-(4-Nitrophenyl)ethyl]-2′-O-acetyl-3′,5′-O-(1,1′,3,3′-tetraisopropyldisiloxane-1,3-diyl)-β-*D*-arabinoguanosine (10).* A solution of compound **9** (100 mg, 0.12 mmol) and LiOAc (50 mg, 0.72 mmol) in *N*,*N*-dimethylformamide (1.2 mL)−hexamethylphosphoramide (0.5 mL) was stirred overnight and poured into ice−water (10.0 mL) to yield a precipitate. This product was filtered off by suction, washed with water, and dried under high vacuum to yield the title compound as a yellow powder: 58 mg (65%). Larger scales produced compound **10** as an orange gum. This was dissolved in ethyl acetate and dried over magnesium sulfate to yield compound **10** as a sticky orange foam. R_f (TLC, toluene−ethyl acetate, 1:1 v/v) 0.5. FAB MS, M + 1 717, M + 2NBA + Na^+ 1157, M calcd 716. ^{1}H NMR ($CDCl_3$) ppm 8.16 (d, 2H, ortho to NO_2), 7.85 (s, H8), 7.48 (d, 2H, meta to NO_2), 6.33 (d, H1′, $J_{1′2′}$ = 6.0 Hz), 5.53 (d, H2′), 4.7 (m, H3′, OCH_2CH$_2$), 4.08 (m, H5′/H5″), 3.87 (m, H4′), 3.27 (t, OCH$_2$CH_2), 1.95 (s, acetyl CH_3), 1.02 [m, Si−C$H$$(CH_3)_2$ and CH_3 from 4 *i*-Pr).

*(E) N^2-Isobutyryl-O^6-[2-(4-nitrophenyl)ethyl]-2′-O-acetyl-3′,5′-O-(1,1′,3,3′-tetraisopropyldisiloxane-1,3-diyl)-β-*D*-arabinoguanosine (11).* To a solution of **10** (170 mg, 0.23 mmol) in absolute pyridine (5 mL) was added 4-DMAP (5 mg) followed by isobutyryl chloride (25 μL, 0.25 mmol). After being stirred for 30 min, the reaction mixture was evaporated to dryness, and the residue was taken up in EtOAc. The organic layer was washed sequentially with saturated $NaHCO_3$ and brine and dried (magnesium sulfate) to give an oil. Further coevaporation steps with toluene, followed with dichloromethane and ether, gave the title compound as a light orange foam: yield 160 mg (90%). Note: when isobutyrylation was attempted with isobutyric anhydride [(*i*-Bu)$_2$O] instead of *i*-BuCl, no reaction occurred even in the presence of the 4-DMAP catalyst, and 6 additional equivalents of the anhydride (room temperature, 3 days). R_f of compound **11** (TLC, dichloromethane−ethyl acetate, 1:1 v/v) 0.75. FAB MS, M^+ 787, M calcd 787. ^{1}H NMR ($CDCl_3$) ppm 8.14 (d, 2H, ortho to NO_2), 8.03 (s, NH), 7.78 (s, H8), 7.49 (d, 2H, meta to NO_2), 6.64 (d, H1′, J = 6.5 Hz), 5.52 (d, H2′), 4.8 (m, H3′), 4.68 (t, OCH_2CH$_2$), 4.08 (m, H5′/H5″), 3.87 (d, H4′), 3.09 (t, OCH_2CH$_2$), 1.69 (s, CH_3 from acetyl), 1.20 (d, *i*-Pr), 1.02 [m, Si−C$H$$(CH_3)_2$ and CH_3 from 4 *i*-Pr].

*(F) N^2-Isobutyryl-O^6-[2-(4-nitrophenyl)ethyl]-2′-O-acetyl-β-*D*-arabinoguanosine (12).* To a solution of nucleoside **11** (1.2 g, 1.52 mmol) in anhydrous tetrahydrofuran (35.0 mL) was added glacial acetic acid (0.68 mL, 11.4 mmol) followed by 1.0 M tetra-*n*-butylammonium fluoride in tetrahydrofuran (9.1 mL, 9.1 mmol). After being stirred for 1 day, ethyl acetate (120 mL) was added, and the resulting mixture washed with saturated $NaHCO_3$ and brine. A light yellow foam was obtained upon evaporation of the organic layer. This crude material (80% yield) may be used without purification in the synthesis of compound **13**. Purification by flash chromatography (dichloromethane−methanol, gradient 1:0 to 19:1 v/v) led to considerable decomposition of the title compound (12% yield). R_f (TLC, $CHCl_3$−MeOH,

19:1 v/v) 0.1. FAB MS, M + 1 545, M calcd 545. ^{1}H NMR ($CDCl_3$) ppm 8.15 (d, 2H, ortho to NO_2), 8.07 (s, NH), 7.9 (s, H8), 7.5 (d, 2H, meta to NO_2), 6.5 (s, H1′, J = 6.5 Hz), 5.36 (d, H2′), 4.77 (m, H3′, OCH_2CH_2), 4.0 (m, H4′), 3.9 (H5′ and H5″), 3.3 (t, OCH_2CH_2), 1.73 (s, CH_3 from acetyl).

*(G) N^2-Isobutyryl-O^6-[2-(4-nitrophenyl)ethyl]-2′-O-acetyl-5′-O-(monomethoxytrityl)-β-*D*-arabinoguanosine (**13**).* A mixture of nucleoside **12** (2.2 g, 4.6 mmol) and monomethoxytrityl chloride (2.12 g, 6.9 mmol) in pyridine (40 mL) was stirred overnight. The next day more monomethoxytrityl chloride (0.5 g) was added, and the reaction was allowed to proceed for another 16 h. After addition of ethyl acetate (50 mL), the mixture was evaporated at reduced pressure and worked up as for compound **11**. Purification by flash column chromatography (MeOH−CH_2Cl_2, gradient 0:1 to 1:19 v/v) yielded the title compound as a light yellow foam: 2.59 g (69%). R_f (TLC, MeOH−CH_2Cl_2, 1:10 v/v) 0.52. FAB MS, M^+ 817, M calcd 817. ^{1}H NMR ($CDCl_3$) ppm 8.17 (d, 2H ortho to NO_2), 7.95 (s, NH), 7.86 (s, H8), 7.51 (d, 2H meta to NO_2), 6.8−7.5 (aromatic), 6.66 (s, H1′, $J_{1'2'}$ = 4.5 Hz), 5.29 (d, H2′), 4.79 (t, OCH_2CH_2), 4.59 (m, H3′), 4.08 (m, H5′), 4.17 (d, H4′), 3.78 (s, OMe, trityl), 3.47 (m, H5′/H5″), 3.32 (m, OCH_2CH_2), 1.78 (Me from acetyl).

*(H) N^2-Isobutyryl-O^6-[2-(4-nitrophenyl)ethyl]-2′-O-acetyl-3′-O-(N,N-diisopropyl-β-cyanoethylphosphoramidite)-5′-O-(monomethoxytrityl)-β-*D*-arabinoguanosine (**4a**).* *N*,*N*-Diisopropyl-β-cyanoethylphosphonamidic chloride (35 μL, 1.05 equiv) was slowly added to a solution of nucleoside **13** (0.12 g, 0.15 mmol) and *N*,*N*-diisopropylethylamine (356 μL, 2.0 mmol) in tetrahydrofuran (2 mL). The reaction turned cloudy after being stirred for 15 min. After 1 h (as indicated by TLC, the reaction was virtually complete) the mixture was poured into ethyl acetate (20 mL, prewashed with 5% aqueous $NaHCO_3$) and washed successively with saturated $NaHCO_3$ and brine. The ethyl acetate layer was dried (magnesium sulfate) and concentrated, and the product was isolated by chromatography on a silica gel column with a solvent of hexanes−dichloromethane−triethylamine (50:45:5 v/v/v). Yield 96 mg of a white foam (64%). R_f (TLC, ethyl acetate−triethylamine, 19:1 v/v) 0.84 and 0.76. FAB MS, M^+ 1017, M calcd 1017. ^{31}P NMR (acetone-d_6) ppm 150.69, 150.91 (85% H_3PO_4 as external reference).

*(I) N^2-Isobutyryl-2′-O-acetyl-5′-O-(monomethoxytrityl)-β-*D*-arabinoguanosine (**14**).* To a solution of compound **13** (367 mg, 0.45 mmol) in anhydrous pyridine (8 mL) was added DBU (683 mg, 4.5 mmol). After 12 h, the reaction was worked up by adjusting the pH to 6.0 with 1 N aqueous acetic acid and evaporating to dryness. The crude was taken in dichloromethane (30 mL), extracted with sodium bicarbonate (5% in water), dried over sodium sulfate, and evaporated. The compound was purified by flash column chromatography using dichloromethane−methanol (50:0 to 49:1 gradient) to yield the desired product as a colorless foam (190 mg, 75%). R_f (TLC, chloroform−ethyl acetate−ethanol, 50:45:5 v/v/v) 0.21. FAB MS, M^+ 668, M calcd 667.7. ^{1}H NMR ppm (DMSO-d_6) 12.09 (s, N−H), 11.64 (br s, N−H), 6.83−7.83 [m, 15 H, (C8)−H and MMT], 6.35 (d, H1′, $J_{1',2'}$ = 6 Hz), 5.89 (d, C3′-OH, $J_{3',OH}$ = 5 Hz), 5.18 (dd, H2′, $J_{2',3'}$ = 5 Hz), 4.41 (m, H3′), 4.09 (m, H4′), 3.73 (s, CH_3O−), 3.24−3.44 (m, H5′, H5″), 2.74 [m, CH(CH_3)$_2$ from isobutyryl], 1.70 (s, CH_3 from acetyl), 1.10 [d, (CH_3)$_2$CH− from isobutyryl].

*(J) N^2-Isobutyryl-2′-O-acetyl-3′-O-(N,N-diisopropyl-β-cyanoethylphosphoramidite)-5′-O-(monomethoxytrityl)-β-*D*-arabinoguanosine (**4b**).* To a solution of **14** (150 mg, 0.224 mmol) in THF (anhydrous, 2 mL) was added *N*,*N*-diisopropylethylamine (100 μL, 0.539 mmol) followed by *N*,*N*-diisopropyl-β-cyanoethylphosphoramidic chloride (60 μL, 0.269 mmol). The reaction turned cloudy after 15 min. Prewashed ethyl acetate was added to stop the reaction, which was worked up by washing with sodium bicarbonate (5% in water) and drying over sodium sulfate. The organic layer was evaporated, and the crude was purified by column chromatography (dichloromethane−hexanes−triethylamine, 50:45:5 v/v/v) to afford the desired product as a colorless foam (125 mg, 65%). R_f (TLC, dichloromethane−hexanes−triethylamine, 50:45:5 v/v/v) 0.35, 0.40. FAB MS, M + Na^+ 890, calcd 891. ^{31}P NMR (acetone-d_6) ppm 151.04, 150.41 (85% H_3PO_4 as external reference).

Oligonucleotide Synthesis. Oligoarabinonucleotides were synthesized on an Applied Biosystems 381A synthesizer using standard phosphoramidite chemistry and 3′-araN-LCAA-CPG (500 Å) solid supports (*26*). Arabinonucleoside monomers were dissolved to 0.11 M (araC, araA, araU, araT, and araI) or 0.15M (araG) in anhydrous acetonitrile. Prior to chain assembly, the solid support (1 μmol) was treated with the capping reagents acetic anhydride−*N*-methylimidazole−4-(dimethylamino)pyridine. Chain assembly of sequences was carried out as follows: (i) Detritylation: 3% trichloroacetic acid in dichloroethane delivered in 100 s (+40 s "burst") steps. The eluate from this step was collected and the absorbance at 478 nm (MMT+) measured to determine the average coupling reaction yield (ca. 90%). (b) Nucleoside phosphoramidite coupling time of 7.5 min. (c) Capping: 1:1 (v/v) of acetic anhydride−collidine−THF, 1:1:8 (solution A), and 1-methyl-1*H*-imidazole−THF, 16:84 (solution B), delivered in 15 s + 35 s "wait" steps. (d) Oxidation: 0.2 M iodine in THF−water−pyridine, 7:2:1, delivered in 20 s + 35 s wait steps. Couplings efficiencies as determined by trityl color analysis were 60−100%. The 5′-terminal trityl group was removed by the synthesizer, and the oligomers were then removed from the support and deprotected by treatment of the CPG with a solution containing concentrated ammonium hydroxide−ethanol (3:1 v/v; 1 mL) for 2 days at room temperature. The ammonium hydroxide−ethanol solution was evaporated and the crude product purified by preparative polyacrylamide gel electrophoresis (PAGE) followed by gel filtration (desalting) on a Sephadex G-25 column (*27*).

Oligonucleotides containing araG were prepared using monomers **1**, **2**, **3**, and **4a**. Oligomers containing araG^{iBu,NPE} or araI^{NPE} units were subjected to an additional deprotection step; that is, following the ammonia treatment and evaporation steps, the oligomer was treated with a solution of 1 M tetra-*n*-butylammonium fluoride in tetrahydrofuran (15 μL per araG or araI residue, room temperature, 16 h). This step cleaves the *p*-nitrophenylethyl protecting group at the O6-position of guanine and hypoxanthine residues (note: the reagent $Et_3N{\cdot}HF$ does not effect the removal of NPE groups). This solution is then quenched with water (1 mL) and desalted via size exclusion chromatography (Sephadex G-25 column). Purification is then carried out by gel electrophoresis as described above and the molecular weight confirmed by MALDI-TOF mass spectrometry.

Scheme 1[a]

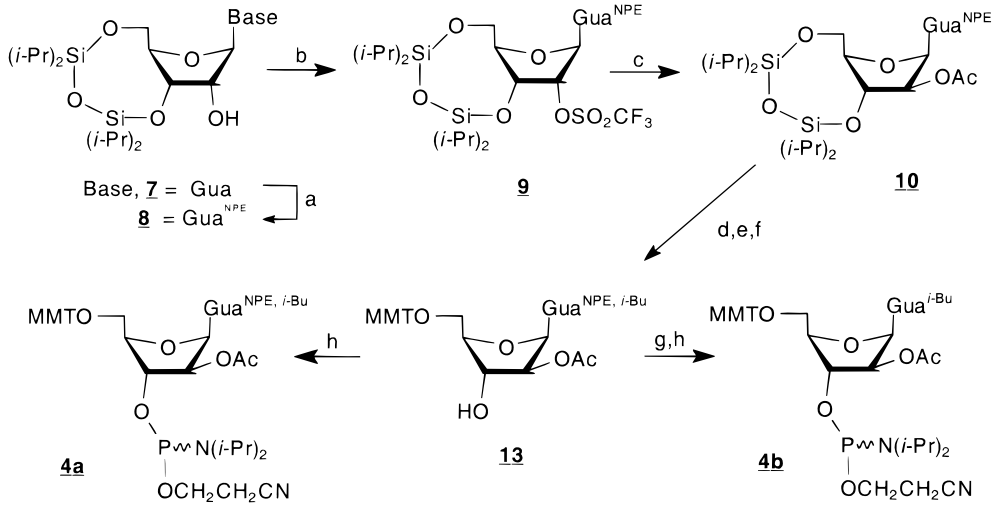

[a] Reactants: *p*-nitrophenylethanol, $(EtCO_2N)_2$, Ph_3Ph, THF, 4 h (73%); (b) Tf_2O, CH_2Cl_2, pyridine, 0 °C, 1 h (82%); (c) LiOAc, HMPA, DMF, 16 h; (d) *i*-BuCl, 4-DMAP, pyridine, 30 min (90%); (e) TBAF/AcOH (6:7.5 v/v), THF (crude: 80%); (f) MMT-Cl, pyridine, 24 h (69%); (g) DBU, pyridine, 12 h (75%); (h) Cl−P(OCE)N(*i*-Pr)$_2$, EtN(*i*-Pr)$_2$;THF (65%).

Oligoribonucleotides were assembled on the same instrument using silyl phosphoramidite chemistry as previously described (*27*). DNA and PS-DNA oligomers were obtained commercially (Dalton Chemical Laboratories, Inc., Toronto, and University of Calgary DNA Synthesis Laboratory, Calgary).

RNase H Induction Assays. The ability of oligonucleotides to elicit RNase H degradation of target RNA was determined in assays (10 μL final volume) that comprised 1 pmol of 5′-^{32}P-labeled target RNA and 2−5 pmol of test oligonucleotide in 60 mM Tris-HCl (pH 7.8) containing 2 mM dithiothreitol, 60 mM KCl, and either 10 mM $MgCl_2$ or 0.1 mM $MnCl_2$. Following preincubation at indicated temperatures for 15−30 min, reactions were started by the addition of 5−20 ng of HIV-1 reverse transcriptase (RT) or 0.1−1.0 unit of *E. coli* RNase H (Pharmacia, Quebec, or Life Technologies, Frederick, MD) as indicated in the legends of Figures 3 and 4. Reactions were stopped by the addition of loading buffer (98% deionized formamide, 10 mM EDTA, 1 mg/mL bromophenol blue, 1 mg/mL xylene cyanol) and heating at 100 °C for 5 min. The reaction products were resolved by electrophoresis using a 16% polyacrylamide sequencing gel containing 7 M urea and visualized by autoradiography.

Nuclease Resistance Assays. Oligonucleotides were 5′-end-labeled with [γ-^{32}P]ATP and gel purified on 16% polyacrylamide sequencing gel. The specific radioactivities of all of the oligonucleotides tested were normalized by mixing with excess cold oligonucleotides. Snake venom phosphodiesterase (SVPDE) digestions were carried out at 37 °C in 70 μL aliquots containing 100 mM NaCl, 10 mM $MgCl_2$, and 100 mM Tris-HCl (pH 8.9), 100 nM oligonucleotides, and 0.001 unit of SVPDE (Amersham Pharmacia Biotech, Piscataway, NJ). For assays of the stability in serum, 100 nM oligonucleotides were incubated with 90% human serum (Sigma, St. Louis, MO) at 37 °C. At the indicated time intervals, aliquots were taken and stopped by loading buffer. The digestion mixtures were then resolved on a 16% polyacrylamide sequencing gel containing 7 M urea in 0.5× TBE buffer.

RESULTS

Synthesis of Arabinonucleoside Building Blocks. We earlier reported procedures for the synthesis of 5′-monomethoxytritylated arabinonucleoside building blocks (araU, araC^{Bz}, and araA^{Bz}) by the phosphoramidite method, based on a highly regiospecific phosphitylation of the 3′-hydroxyl group (*20*−*22*). In an effort to extend this method to the preparation of oligoarabinonucleotides with mixed base composition, we now report on the synthesis of the corresponding araG, araI, and araT 3′-phosphoramidite monomers.

The synthesis reported below for araG (N2^{iBu}, O6^{NPE}) is based on the procedure of Resmini and Pfleiderer (*28*), in which riboG is converted to araG by triflating the 2′-OH group followed by S_N2 displacement at C2′ with LiOAc. Our synthetic strategy differs primarily in the choice of sugar and N^2-protecting groups. Instead of the acetyl group, we used Markiewicz's disiloxane group (*29*) to regiospecifically mask the 5′- and 3′-hydroxyl groups, leaving the 2′-hydroxyl group free for sulfonylation (triflation) (see Scheme 1). However, before this step can be carried out, the heterocyclic base must be protected with the *p*-nitrophenylethyl group (NPE) to prevent potentially troublesome reactions at the lactam moiety (*28*, *30*). Thus, a mixture of triphenylphosphine and diethyl azodicarboxylate was added to nucleoside **7** to afford riboG^{O6-NPE} (**8**) in 73% yield. Transient 2′-triflation with trifluoromethanesulfonic anhydride (giving **9**) followed by displacement at C2′ using LiOAc gave the 2′-O-acetylated araG^{O6-NPE} (**10**) in moderate yield (50%). If desired, the 2′-O-triflate riboG^{O6-NPE} intermediate **9** can be isolated by silica gel column chromatography, but the conditions required can lead to significant loss of material. Instead, it is best to use the crude **9** in the ensuing reaction with LiOAc.

NMR data of compounds **9** and **10** are in accordance with earlier observations made by Robins (*31*) and Pfleiderer (*28*) that a 5′,3′-disiloxane moiety "locks" the furanose ring in the C3′-endo conformation (e.g., large $J_{3',4'}$ coupling constant). The splitting of the anomeric (H1′) NMR signal observed for these compounds is typical for ribo (**9**, $J_{1',2'}$ =

0−1.5 Hz) and arabino (**10**, $J_{1',2'} = 6-6.5$ Hz) nucleosides adopting the C3′-endo geometry, confirming the stereochemistries at C2′.

Protection of the guanine exocyclic amino group with isobutyryl chloride was postponed to a later stage to avoid depurination during the 2′-triflation step (*28*). This side reaction appears to be favored for araG protected at both the O^6 atom (NPE) and the exocyclic amino group (*i*-Bu). Selective removal of the disiloxane moiety with tetrabutylammonium fluoride−AcOH followed by 5′-monomethoxytritylation and 3′-phosphitylation gives the O^6-NPE protected monomer **4a** in an overall yield, from guanosine, of 22%. Alternatively, the O^6-NPE group may be removed prior to the final 3′-phosphitylation reaction to afford the (O^6-free) guanosine derivative **4b**. By a similar strategy, araI was converted in six steps to the *O*^{6}-*p*-nitrophenylethyl-β-D-arabinoinosine derivative **5** in ca. 30% overall yield from araI (see Supporting Information). The site of phosphitylation (at 3′) was established from the measured two-bond $^2J_{H3'-P}$ and three-bond $^3J_{H2'-P}$ coupling constants (ca. 11 and 0.8 Hz, respectively).

Finally, araT phosphoramidite **6** was prepared from readily available 2,3,5-tri-*O*-benzoyl-1-*O*-acetyl-α-D-ribose (Supporting Information). Vorbrüggen coupling of this sugar with thymine followed by debenzoylation using aqueous ammonia afforded ribothymidine with the heterocyclic base attached specifically in the β configuration (*32*). Reaction with monomethoxytrityl chloride to give 5′-MMT-rT followed by treatment with diphenyl carbonate (130 °C, 2 h) and ethanolic KOH (room temperature, 16 h) gives 5′-MMT araT (*22*, *33*). In the last two steps, phosphitylation at the sterically less hindered 3′-hydroxyl group followed by 2′-acetylation affords the desired araT monomer (**6**) in good yield (*20*−*22*). Structural assignments were based on the UV, FAB-MS, and NMR spectra (*22*).

Oligonucleotide Synthesis. Oligonucleotides were synthesized on a controlled pore glass solid support using standard phosphoramidite protocols (*27*), except that coupling times of 7−8 min were employed for arabinonucleoside units. The coupling efficiencies, based on the absorbance of the monomethoxytrityl cation released after each coupling, were consistent with those observed for RNA synthesis and varied between 80% and 110%. The "110%" yields are probably related to the accuracy of the trityl assay (±5%) or to solid support surface interactions. Deprotection conditions of oligoarabinonucleotides lacking guanine and hypoxanthine were similar to those employed in DNA synthesis. Oligomers containing araG^{iBu,NPE} or araI^{NPE} units were subjected to an additional deprotection step; that is, following the ammonia treatment, the oligomer was treated with a solution of 1 M tetra-*n*-butylammonium fluoride in THF (16 h) to effect the cleavage of *O*^{6}-*p*-nitrophenylethyl protecting groups. Oligonucleotides were purified by polyacrylamide gel electrophoresis followed by size exclusion chromatography. The identity of oligonucleotides was verified by MALDI-TOF mass spectrometry.

Thermal Stability of ANA/RNA and ANA/DNA Duplexes. The binding affinity of various oligoarabinonucleotides to their complementary single-stranded DNA and RNA targets was evaluated in a buffer containing 140 mM KCl, 1 mM $MgCl_2$, and 5 mM Na_2HPO_4 (pH 7.2), which is representative of intracellular conditions. These oligomers, 18 nt in length, are complementary to portions of HIV-1 genomic RNA (Tables 1 and 2). To assess the effects of araI vs araG, and araU vs araT, substitutions, the association properties of ANA sequences **III**−**V** were investigated (Table 1). The incorporation of araT was an obvious choice given the well-known stabilizing effect of thymine and other 5-substituted pyrimidine residues (relative to uracil) (*34*−*36*) and the fact that araU/rA base pairs, unlike rU (or dU)/rA pairs, are unstable (*22*, *37*). For instance, $araU_{10}$ will not form a duplex with its Watson−Crick RNA (rA_{10}) or DNA (dA_{10}) complements (*22*). AraI was used in place of araG in order to compare the relative stabilities of araI/rC versus araG/rC pairs. We also investigated a DNA strand containing an araA insert (**II**, Table 1) in order to assess the effects of a single D-arabinose substitution on DNA/DNA and DNA/RNA duplex stability. As a comparison, the hybridization properties of S-DNA and unmodified DNA and RNA sequences were also investigated. Some of the thermal dissociation data (T_m, % *H*) for the complexes formed are presented in Tables 1 and 2. The key observations can be summarized as follows:

(a) Both DNA/DNA and DNA/RNA duplexes can accommodate a single araA/dT (rU) base pair with only a small loss of stability; the destabilizing effect appears to be greater for the araA/dT pair ($\Delta T_m = -1.8$ °C) than for the araA/rU pair ($\Delta T_m = -0.6$ °C). The apparent destabilization caused by the araA unit is significantly smaller than that created by a mismatch at the same position (ΔT_m = ca. −5 °C), suggesting that the araA residue in these duplexes retains classical base-pairing interactions. This conclusion is also evident from the work of Mikita and Beardsley (*38*), who found that duplex DNA and DNA/RNA hybrids could accommodate an araC/dC (rG) base pair with only a moderate loss of stability.

Table 1: Melting Temperatures (T_m) of Duplexes[a]

code	designation (AON)	sequence	T_m (°C) RNA target	T_m (°C) DNA target
I	DNA	5′-AGC TCC CAG GCT CAG ATC-3′	72.3	68.0
II	DNA/araA	5′-AGC TCC CAG GCT C*a*AG ATC-3′	71.7	66.2
III	ANA (U,G)	5′-AGC UCC CAG GCU CAG AUC-3′	44.0	≈26[b]
IV	ANA (U,I)	5′-AIC UCC CAI ICU CAI AUC-3′	46	≈27
V	ANA (T,I)	5′-AIC TCC CAI ICT CAI ATC-3′	48	≈27
VI	S-DNA	5′-AGC TCC CAG GCT CAG ATC-3′	62.4	58.7
VII	RNA	5′-AGC UCC CAG GCU CAG AUC-3′	84.6	66.2

[a] The melting temperatures (T_m) were obtained as the maxima of the first derivative melting curves (A_{260} vs temperature). All duplexes were 2.3 μM in concentration. Buffer: 140 mM KCl, 1 mM $MgCl_2$, 5 mM Na_2HPO_4 (pH = 7.2). [b] Broad transition and small hyperchromicity observed.

Table 2: T_m Values of Duplexes Formed between Target RNA and Complementary DNA, Thioate-DNA, ANA, and RNA Oligomers[a]

code	designation (AON)	DNA target T_m (°C)	DNA target % *H*	RNA target T_m (°C)	RNA target % *H*
VIII	DNA	50.3	16.6	51.3	17.3
IX	thioate-DNA	37.3	16.4	38.1	13.3
X	ANA	<16	≈4	32.1	10.1
XI	RNA	27.7	15.1	54.2	16.6

[a] Aqueous solutions 2.3 μM in each oligonucleotide, 140 mM KCl, 1 mM $MgCl_2$, 5 mM Na_2HPO_4 buffer (pH 7.2). Sequence of AON oligonucleotides: 5′-TTA TAT TTT TTC TTT CCC-3′ (for ANA and RNA, T is replaced by U).

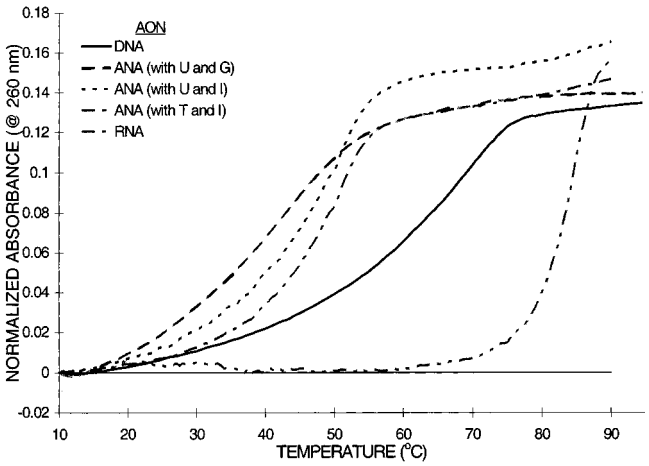

FIGURE 1: Thermal melting curves of oligonucleotides (AON) hybridized to complementary single-stranded RNA. See Table 1 for base sequences. Buffer: 140 mM K^+, 1 mM Mg^{2+}, and 5 mM Na_2HPO_4, pH 7.2.

(b) ANA/RNA hybrids had a lower value of T_m, compared to the corresponding DNA/RNA and RNA/RNA duplexes (Figure 1). The exception appears to be the araA_n/rU_n duplex since it had the same stability as the dA_n/rU_n and rA_n/rU_n controls ($n = 8$, 18) (*22*). The ANA mixed-base sequences bound to target RNA with a decrease of 1.0−1.5 °C/base pair relative to the control DNA sequences. Thus, the binding affinity of the mixed-base antisense (AON) sequences toward complementary RNA follow the order RNA > DNA > thioate-DNA > ANA.

(c) Interestingly, substituting araG/rC with araI/rC base pairs in an ANA/RNA hybrid does not appear to be destabilizing. In fact, ANA (U,I) (**IV**) showed an increased T_m and cooperativity compared to ANA (U,G) (**III**) when paired to the RNA target ($\Delta T_m = +2$ °C, Table 1 and Figure 1). This is in contrast to the pairing behavior of analogous DNA strands, where the same dG to dI substitutions are destabilizing. For example, with complementary RNA, the duplex containing DNA (G,T) is significantly more stable (73 °C) than the corresponding DNA (I,T) duplex (57 °C); i.e., $\Delta T = -4$ °C per each G to I substitution. A further increase in T_m and cooperativity was observed for the sequence ANA (I,T) (**V**) relative to ANA (I,U) (**IV**) when paired to the RNA target ($\Delta T_m = +2$ °C).

(d) An ANA/RNA hybrid containing a single araC/rU mismatch is less stable than the corresponding fully paired ANA/RNA hybrid ($\Delta T_m = -16$ °C). The T_m decrease per dC/rU mismatch within the natural DNA/RNA hybrids is also ca. −16 °C. From this we conclude that ANA and DNA sequences display similar specificities toward a singly mismatched RNA strand.

(e) ANA strands associate weakly (if at all) to single-stranded DNA (ssDNA). For example, complex formation between ANA **III** (or **X**) and complementary ssDNA could not be observed (Tables 1 and 2). An exception appears to be homopolymeric araA_n, which forms a stable complex with both complementary ssDNA and RNA (*22*, *39*).

CD Spectra of ANA/RNA Duplexes. Circular dichroism (CD) is a powerful technique for studying nucleic acid structure, particularly the helical arrangement of double helices (*40*−*42*). B-form helices display a positive band centered near 275 nm, a negative band near 240 nm, and a crossover signature at ca. 260 nm. The latter corresponds to the wavelength maximum of the UV absorption spectrum. In contrast, A-form duplexes exhibit a strong band centered around 260 nm and a fairly intense negative band around 210 nm. This is exemplified by the CD spectra of the reference duplexes DNA/DNA (B-form) and RNA/RNA (A-form) shown in Figure 2 (panel A). Natural DNA/RNA hybrids adopt a more complex sequence-dependent structure that generally resembles the A-helical form. Structurally, this heteroduplex conformation is closer to the A-form of RNA/RNA duplexes and thus is commonly described as an "A-like" helical structure. In agreement with this notion, the spectra of DNA/RNA hybrids shown in Figure 2 very closely resemble the spectrum of the A-form RNA/RNA duplex. The major difference lies in the strength of the negative band at 210 nm, which is much reduced in the DNA/RNA spectra, in comparison with the same band in the RNA/RNA spectra. As shown in Figure 2, panel A, the CD spectra of the ANA (**III**)/RNA hybrid closely resembled the spectra of the DNA/RNA hybrid, suggesting that they share the same A-like helical conformation. Since the A-like hybrid conformation appears to be important in the recognition of nucleic acid duplexes by RNase H (*11*), we studied the susceptibility of ANA/RNA heteroduplexes to cleavage by RNase H. Both *E. coli* RNase H and HIV-1 RT-associated RNase H were examined.

Induction of RNase H Activity by Arabinonucleic Acids. We first examined the susceptibility of heteroduplex ANA (**III**)/RNA to the action of RNase H (*E. coli* and HIV-1 RT), along with the corresponding DNA (**I**)/RNA, and RNA (**VII**)/RNA controls (sequences shown in Table 1). The synthetic RNA target is identical in sequence to a portion of the R region of HIV-1 RNA and exactly complementary to the antisense ANA and control oligonucleotide sequences. To assess the ability of these oligomers to stimulate RNase H activity, the 5′-^{32}P-labeled RNA target and a 3-fold excess of the test oligomer (ANA, DNA, or RNA) were incubated in a buffer containing 2 mM dithiothreitol, 60 mM KCl, and either 10 mM $MgCl_2$ or 0.1 mM $MnCl_2$. Reactions were started by the addition of either HIV-1 RT associated RNase H or *E. coli* RNase H1, and the degradation of the 5′-^{32}P-labeled RNA target was then monitored by polyacrylamide gel electrophoresis. As shown in Figure 3, the control DNA oligomer promoted essentially complete degradation of the 5′-^{32}P-labeled RNA. Cleavage appeared to be specific since a random DNA mixed-base sequence, 18 nt in length [DNA (random)], did not promote degradation of the target RNA. The two bands appearing below the target RNA are found even in the absence of any oligomer (compare lanes DNA random and no AON) and are minor contaminants of the synthetic 5′-^{32}P-labeled octadecaribonucleotide. As expected, neither the RNA/RNA duplex nor the 5′-^{32}P-labeled RNA alone served as substrates for RNase H. With ANA and HIV-1 RT RNase H, only partial degradation of target RNA was observed, although significantly more cleavage occurred with Mn^{2+} than with Mg^{2+}. Of note, when the hybrid ANA/5′-^{32}P-labeled RNA and *E. coli* RNase H1 were incubated in the buffer containing Mn^{2+}, nearly complete degradation of the target 5′-^{32}P-labeled RNA was observed (Figure 3). This result clearly confirms previous observations that while both Mg^{2+} and Mn^{2+} can activate RNase H, there are

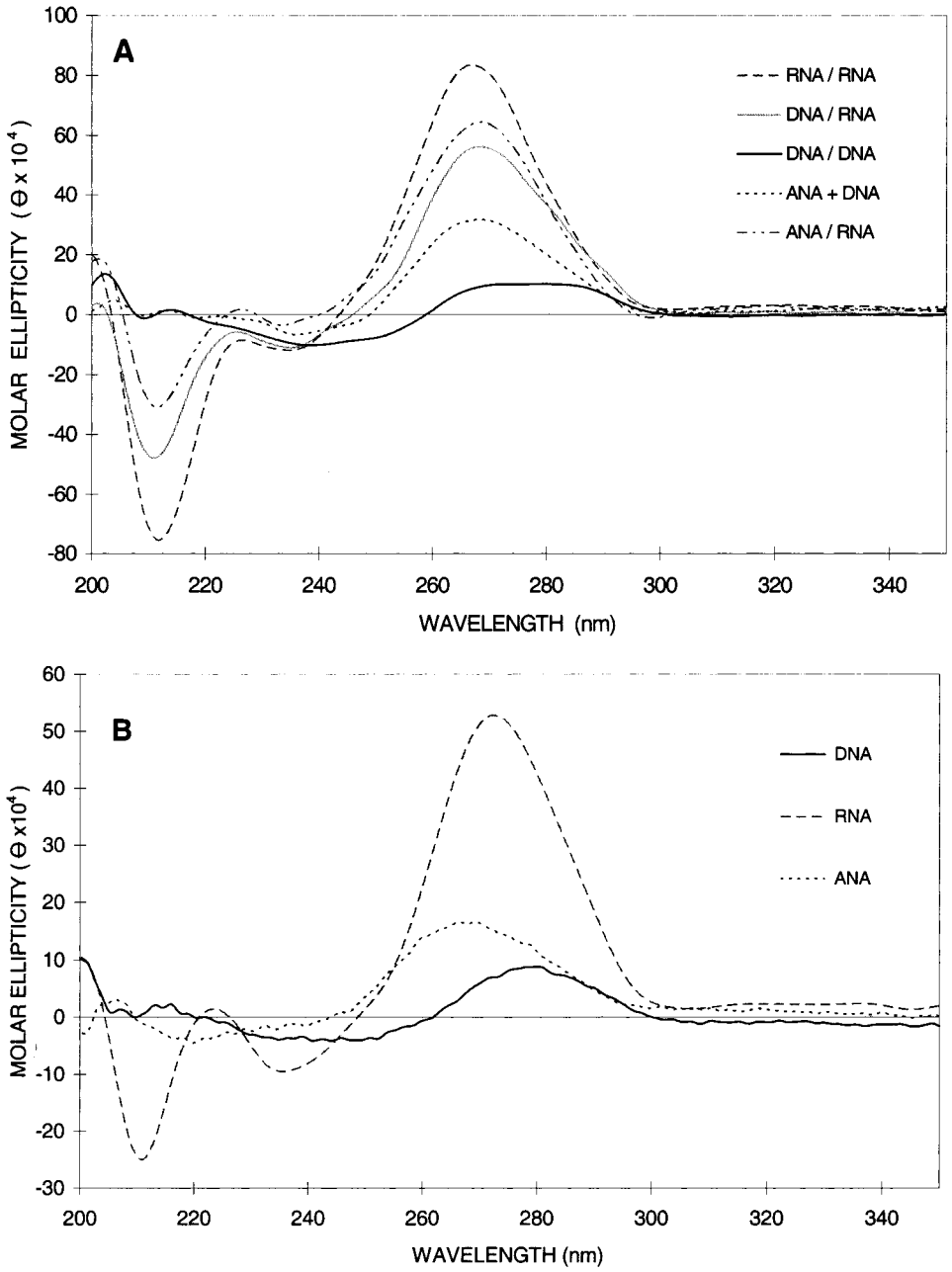

FIGURE 2: Circular dichroic (CD) spectra of (A) duplexes and (B) free single strands. Buffer: 140 mM K^+, 1 mM Mg^{2+}, and 5 mM Na_2HPO_4, pH 7.2. See Table 1 for base sequences and Materials and Methods for experimental conditions. ANA refers to oligomer ANA (U,G) **III** (Table 1).

significant differences between the effects of these two divalent metals (*43*).

Similar experiments were carried out with ANA sequence **X** (Table 2). Figure 4 compares the susceptibility of ANA (**X**)/RNA and its corresponding DNA (**VIII**)/RNA and thioate-DNA (**IX**)/RNA duplexes to the action of *E. coli* RNase H1. RNase H activation is evident in all three cases by the numerous smaller sized degradation bands of the target 5′-^{32}P-labeled RNA oligomer. Again, neither the RNA/RNA duplex nor the 5′-^{32}P-labeled RNA alone served as substrates for RNase H. The lack of complete cleavage observed with ANA (**X**) at 39 °C, i.e., 78% cleavage of full-length RNA species (Figure 4, panel A), may reflect (a) the inability of RNase H to bind optimally to the minor groove of ANA/RNA hybrids or (b) the low thermal stability of this particular complex (T_m 32.1 °C; i.e., <50% duplex present at 39 °C). We favor the second notion because ca. 17% more cleavage of the target RNA was observed when the temperature of the RNase H assay was lowered to 25 °C (Figure 4, panel A). Upon further cooling (T = 15 °C), one begins to observe a reduction of RNase H activity (rate of hydrolysis) and a corresponding decrease in RNA degradation (i.e., 95% cleavage at 25 °C and only 70% cleavage at 15 °C).

Enzymatic Hydrolysis. Next we studied the behavior of homopyrimidine sequences with respect to their enzymatic stability against snake venom phosphodiesterase I (SVPDE). SVPDE is an aggressive enzyme that rapidly degrades single-stranded nucleic acids via 3′-exonuclease activity. Since 3′-exonuclease activity is the major source of degradation of DNA and RNA oligomers in serum, it seemed appropriate to study the susceptibility of 5′-^{32}P-labeled oligomers against the action of this readily available enzyme (SVPDE).

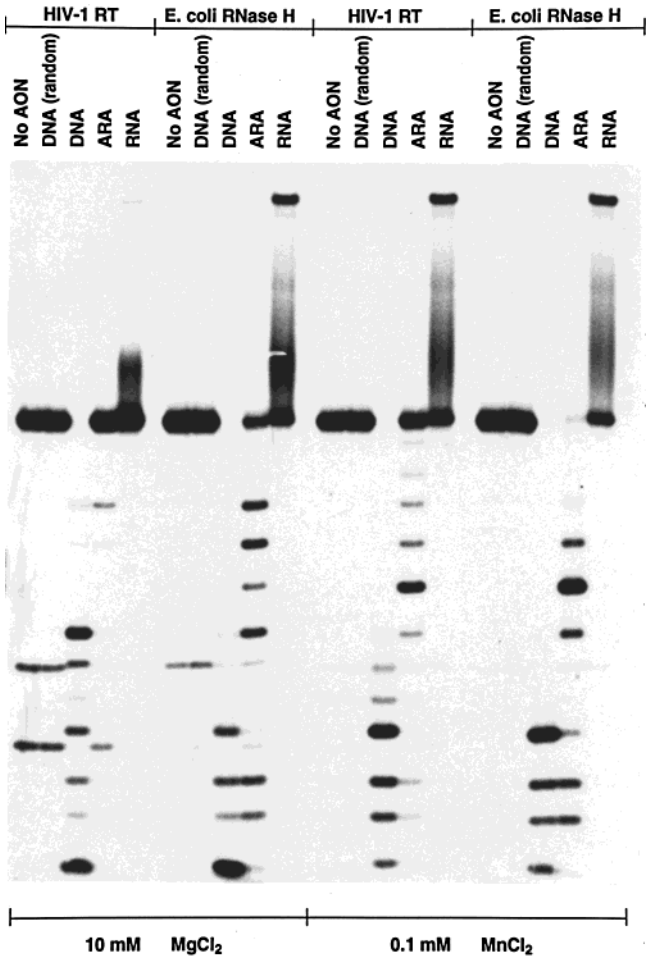

FIGURE 3: Ribonuclease H degradaton of various 18-bp oligonucleotide hybrid duplexes. An 18-nt 5′-^{32}P-labeled target RNA (5′-GAU CUG AGC CUG GGA GCU-3′) was preincubated with complementary 18-nt DNA **I** (DNA), ANA **III** (ARA), and RNA **VII** (RNA), as well as with a noncomplementary DNA sequence (DNA random), and then added to reaction assays containing either HIV-1 RT or *E. coli* RNase H at the indicated divalent cationic metal concentrations. Base sequences of oligomers are given in Table 1. The slowly migrating band in the RNA lanes is the RNA (**VII**)/RNA duplex (T_m 85 °C), which withstands the denaturing conditions of the gel electrophoresis and the heating of the sample to 100 °C prior to being loaded onto the gel. See Materials and Methods for detailed experimental conditions.

Digestion with SVPDE was readily monitored and quantitated by polyacrylamide gel electrophoresis (densitometry); the results are summarized in Figure 5. The order in enzymatic stability against SVPDE for the homopyrimidine series was found to be S-DNA ≫ ANA > 2′F-ANA ≈ RNA > 2′F-RNA > DNA. On the basis of these results, we conclude that arabinonucleic acids are more stable toward SVDPE hydrolysis than the ribonucleic acid derivatives; i.e., ANA > RNA and 2′F-ANA > 2′F-RNA. The data also suggest that as the van der Waals radii of the 2′(β or α) substituent increases, enzymatic stability increases in the same order; i.e., DNA (2′H$_\beta$) < 2′F-ANA (2′F$_\beta$) < ANA (2′OH$_\beta$); similarly, DNA (2′H$_\alpha$) < 2′F-RNA (2′F$_\alpha$) < RNA (2′OH$_\alpha$). The phosphorothioate substitution (S-DNA) resulted in the largest increase in enzymatic stability. The same trends were observed when the oligomers were subjected to degradation using human serum (data not shown). More details on the biochemical and physical properties of 2′F-ANA oligomers will be published elsewhere (Wilds et al., in preparation).

DISCUSSION

Arabinonucleosides are stereo isomers of ribonucleosides, differing only in the configuration at the 2′-position of the sugar ring. They have had a substantial impact on chemotherapy, and as such they have been extensively used as antiviral and anticancer drugs (for a review, see ref *44*). β-D-Arabinofuranosylcytosine (araC) is the most successful nucleoside antileukemic agent and is widely used in combination therapy or at high doses as a single agent to treat patients with acute lymphoblastic and myeloblastic leukemias (*45*, *46*).

Oligonucleotides constructed from arabinonucleotides have been under investigation from various different aspects. Short oligomers of arabinonucleotides have been considered as pro drugs in an attempt to improve the solubility of arabinonucleoside therapeutics (*47*). Incorporation of araC into DNA strands has also been the focus of research to understand the mechanism of action of this anticancer drug (*38*, *48*). In the crystal, DNA duplexes containing araC adopt a normal B-type double helix with only small conformational perturbations at the araC/dG base pair (*49*−*51*). Mikita and Beardsley have prepared DNA/DNA and DNA/RNA duplexes containing a single araC insert and found that both duplexes can accommodate araC/dG (rG) base pairs with only a moderate and equivalent loss of stability (*38*).

The association properties of *uniformly* modified oligoarabinonucleotides (2′OH araN$_n$, N = U, A, and C) were investigated by Giannaris and Damha (*22*) and independently by Kois and Watanabe (2′F-araT$_{11}$ and 2′F-araU$_{11}$) (*52*, *53*). Giannaris and Damha showed that araA$_8$ associated with poly(riboU) and poly(deoxyT); the melting temperature of the resulting complex was slightly higher than the corresponding complexes formed by the normal riboA$_8$ and deoxyA$_8$ strands (*22*). They also showed that araC$_8$ and ara-(UCU UCC CUC UCC C) associated with their complementary RNA strand, *albeit* with lower affinity relative to the corresponding unmodified strands. Also, araU$_8$ did not hybridize with poly(riboA) under conditions where riboU$_8$ and deoxyU$_8$ formed a complex with poly(rA). Watanabe reported that 2′F-araT$_{11}$ and 2′F-araU$_{11}$ oligomers were able to bind to the complementary DNA with equal or slightly better affinity compared to the control dT$_{11}$ (DNA) oligomer (*53*). More recently, Noronha and Damha tested a pyrimidine ANA for its ability to recognize double-helical complexes (*54*). The pyrimidine ANA was shown to form triple-helical complexes with duplex DNA, and hybrid DNA (Pu)/RNA (Pyr), *albeit* with slightly lower affinity compared with the corresponding pyrimidine DNA and RNA strands.

More recent studies have focused on modified DNA strands containing one or a few arabinonucleotide units having a β-amino (*55*), bromo (*56*), ethynyl (*57*), fluoro (*58*, *59*), methyl (*60*), and methoxy (*61*) group at C2′ of the furanose ring. Generally, DNA strands containing these modifications show weaker pairing with complementary DNA or RNA sequences relative to an unmodified DNA. An exception is modified DNA containing 2′F-araT units, which shows enhanced binding with complementary DNA relative to unmodified DNA (*58*).

In the present study we prepared ANA strands containing mixed-base composition, as they are more ideal models for hybridization studies and biological investigations. We find

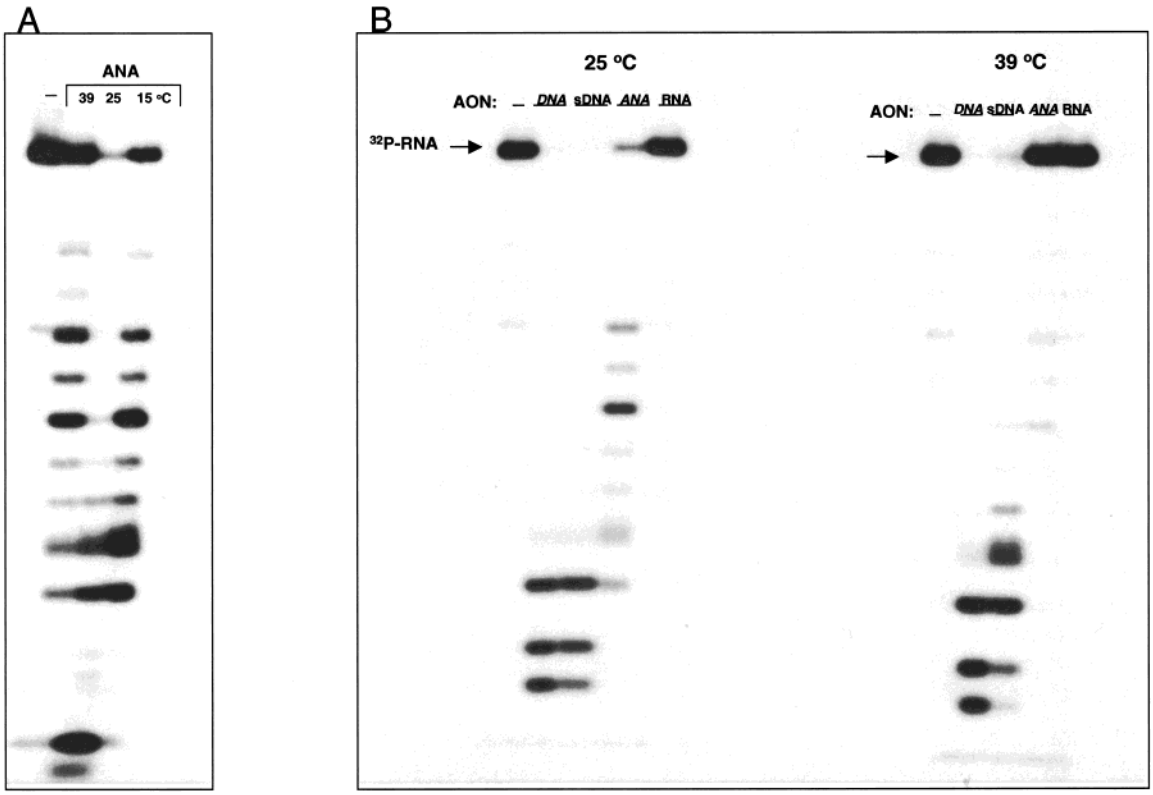

FIGURE 4: Ribonuclease H degradation of various hybrid duplexes as a function of temperature. (A) 5′-^{32}P-GGG AAA GAA AAA AUA UAA-3′ was preannealed with complementary ANA (**X**) for 30 min at the temperatures indicated. Reactions were initiated by adding 1 unit of *E. coli* RNase H and allowed to proceed for 1 h before analysis (buffer: 10 mM $MgCl_2$). (B) An 18-nt 5′-^{32}P-labeled target RNA (5′-GGG AAA GAA AAA AUA UAA-3′) was preannealed at 25 and 39 °C with complementary DNA (**VII**), S-DNA (**IX**), ANA (**X**), or RNA (**XI**) (10 mM $MgCl_2$). *E. coli* RNase H (0.5 unit) was then added, and reactions were allowed to proceed for 30 min before analysis. Base sequences of AON oligomers are given in Table 2.

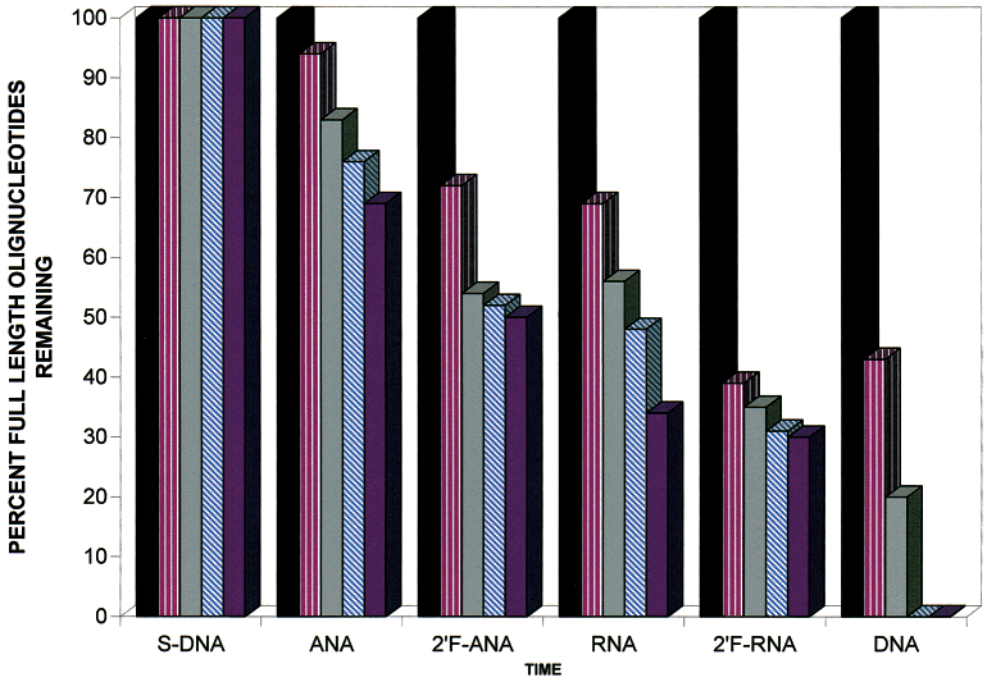

FIGURE 5: Hydrolytic stability of AONs toward snake venom phosphodiesterase (SVPDE). 5′-^{32}P-labeled ANA (araU_{18}), 2′F-ANA (2′F-araT_{18}), DNA (dT_{18}), S-DNA (S-dT_{18}), and RNA (rU_{18}) were digested with SVPDE for a period of 0, 5, 10, 20, and 30 min (*X*-axis), and the amount of full-length AON remaining was quantitated by densitometry (*Y*-axis). See Materials and Methods for detailed experimental conditions.

that they exhibit certain characteristics desirable for use as antisense agents. They form duplexes with complementary RNA, direct RNase H degradation of target RNA molecules, and display resistance to 3′-exonucleases such as snake venom phosphodiesterase, as well as those present in serum.

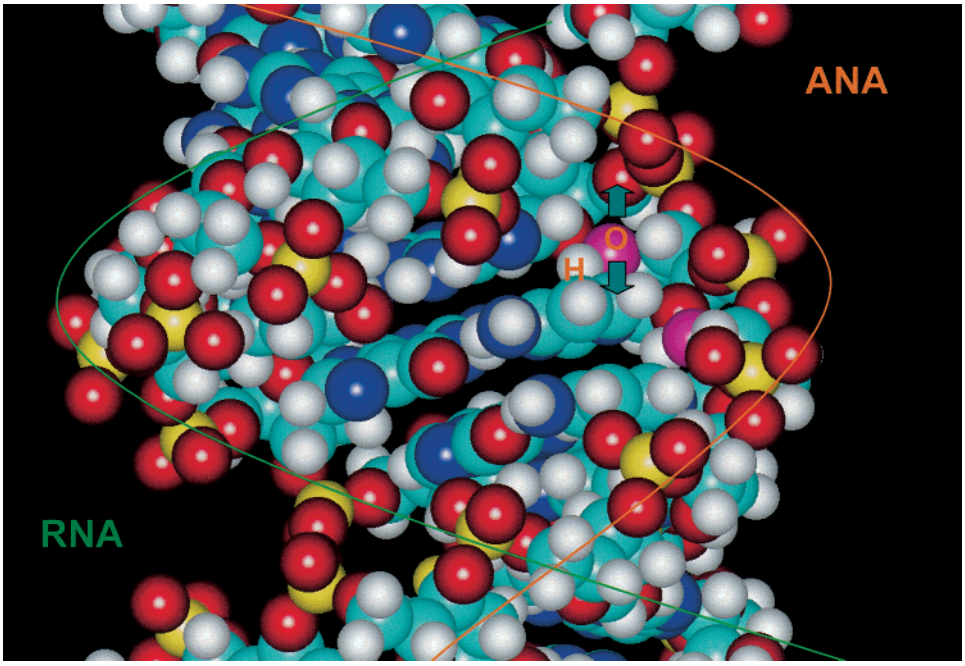

FIGURE 6: Energy-minimized structure of the hybrid duplex ANA (**III**)/RNA. The steric interactions of the arabinose 2′-OH groups (oxygen shown in pink) within the major groove are indicated with arrows. The duplex structure was generated using HyperCube's molecular modeling system (HyperChem, version 5.0) as described previously (*67*).

An indication of the stability of duplexes formed between ANA and their target DNA and RNA was obtained from UV melting profiles. A previous study conducted by our group indicated that the stability of homopolymeric ANA/RNA duplexes was partly influenced by base sequence; e.g., ara(Ap)$_n$A bound to both rU$_n$ and dT$_n$, whereas ara(Up)$_n$U failed to form a complex with either rA$_n$ or dA$_n$ (*22*). In the present study, ANA oligomers of mixed-base composition formed stable duplexes with complementary RNA, although they had lesser binding affinity compared to the natural (DNA, RNA) or thioate-DNA counterparts. The arabino substitution destabilizes a mixed-base ANA/RNA duplex by ca. 1.0−1.5 °C per base pair when compared with native DNA/RNA hybrids (Tables 1 and 2). This destabilization is presumed to derive from steric interference by the β-C2′-OH group, which is oriented into the major groove of the helix, causing slight local deformation, e.g., unstacking (Figure 6) (*48*). Consistent with this notion is the observation that replacing the ara-2′-OH group with a smaller 2′F atom results in a marked increase in duplex melting temperature (*23*). Another explanation has been offered recently by Venkateswarlu and Ferguson (*62*) and reviewed by Manoharan (*3*). Ferguson reported on ANA/RNA conformation by a computational study and concluded that the sugar puckers of ANA strands adopt the C2′-endo geometry. This theoretical study further indicated that the ANA strand is rigid due to the formation of an intramolecular hydrogen bond between the C2′-OH group and the C5′-oxygen of the arabinose sugar, which helps to "lock" the conformation in the C2′-endo form. This feature can be traced back to the properties of monomeric arabinonucleoside residues (araU and araC), in which such interactions have in fact been observed (*63*). This intrasugar hydrogen bond O(2′)−H$\cdots$(5′) would then preorganize the ANA strand to a more B-like conformation, leading to less favorable ANA−RNA interactions in an A-like hybrid geometry.

As expected, an ANA oligomer which incorporates araT residues, in place of araU, was found to have improved binding affinity toward RNA, relative to an ANA sequence containing araU (Table 1). This compares well with observations made earlier for natural DNA sequences and may reflect increased base stacking interactions between thymine and adjacent base pairs ("methyl effect") (*34*−*36*). Interestingly, an ANA oligomer that incorporates araI residues shows equal or better binding affinity toward a target RNA, relative to ANA sequence containing araG residues at the same positions. This implies that ANA substitution is destabilizing for one of the Watson−Crick H-bonds in the G/C base pair. Whether the "destabilizing" effect observed for araG is a general phenomenon that is also valid for other ANA sequences remains to be shown.

In view of the anticipated preorganized, "B-like" character of ANA strands (C2′-endo conformation), it is somewhat unexpected that, with the exception of oligo(araA), ANA strands form weak complexes with complementary ssDNA. These findings most likely reflect major distortions in the normal structure of the B-helix by unfavorable steric interactions involving the arabinose 2′-OH substituent (*60*). Consistent with this notion, substituting 2′-OH groups with the smaller 2′F groups (i.e., 2′F-ANA) restores binding to single-stranded DNA (*39*). Clearly, high-field NMR analysis and crystallographic work on ANA/DNA and ANA/RNA hybrids are needed to gain a better understanding of these effects.

Induction of RNase H activity is likely to have therapeutic value by enhancing the antisense effect relative to oligomers that are unable to activate this enzyme (*6*, *9*). Up to now, RNase H induction by modified oligonucleotides has only been met by thioated DNA (PS- and PS$_2$-DNA), by borano-DNA, and by "gapmers", oligonucleotides consisting of a nonuniform backbone (*1*). An example of gapmers includes chimeras of DNA and 2′-OMe RNA or chimeras of DNA and peptide nucleic acid (PNA), both known to elicit RNase

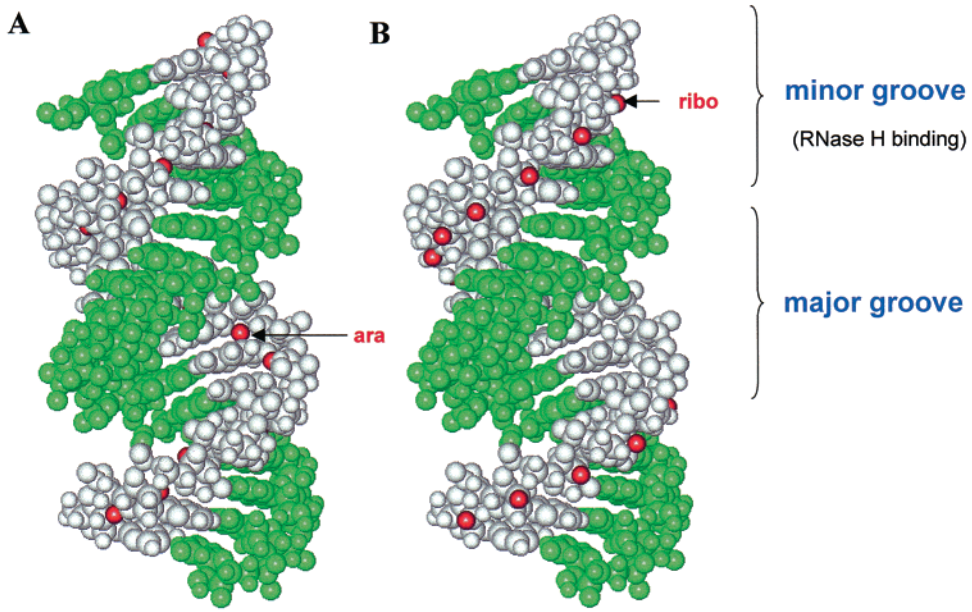

FIGURE 7: Energy-minimized structure of the hybrid duplex DNA (**I**)/RNA (*67*). The green strand represents the target RNA. Prochiral 2′H_β atoms (arabino configuration, major groove) are shown in red in panel A, whereas 2′′H_α atoms (ribo configuration, minor groove) are shown in panel B.

H activity (*1*). The DNA portion or "gap", usually 6−10 bases long, is usually positioned in the middle of the chimera for RNase H recognition and cleavage (*14*, *64*). The present work shows that ANA is capable of directing RNase H degradation of target RNA molecules in a sequence-specific manner. Thus ANA represents the first class of an entirely *2′-modified* oligonucleotide (with phosphodiester linkages) that maintains the ability to induce RNase H activity. This is presumably due to the formation of *A-like* ANA/RNA hybrids that closely mimic the native DNA/RNA structure needed for RNase H cleavage, as evident from our CD studies (Figure 2) (*23*). Recent molecular dynamic simulations conducted by the Ferguson group further corroborate this result (*62*). Their calculations yielded ANA/RNA and DNA/RNA hybrids with strikingly similar minor groove widths, i.e., 14−15 Å (as estimated by interstrand phosphate distance), a value that is intermediate compared to ideal A-form or B-form geometries. This property, taken together with the fact that the 2′OH groups of the ANA strand project into the major groove of the helix (Figure 7), where they should not interfere with RNase H recognition and cleavage, helps to explain the induction of RNase H by ANA/RNA hybrids. Another attractive possibility is that the anticipated "DNA-like" sugar geometry of arabinose (*54*, *62*) plays a role in RNase H activation.

The conclusions drawn from all of this is that minor groove dimensions of the hybrid, as well as the structure (e.g., 2′-stereochemistry) and conformation of the AON, are key determinants in the activation of RNase H. "RNA mimics" (e.g., 2′-*O*-alkyl-RNA, 2′F-RNA, 2′,5′-DNA, α-DNA, or 3′,5′-phosphoramidate-linked DNA) produce duplexes that are too similar to the RNA/RNA duplex and hence are not cleaved by the enzyme. Our results strongly support the notion that activation of RNase H requires a DNA-like oligonucleotide that binds to target RNA to yield duplexes that resemble the native DNA/RNA substrates, e.g., PS-DNA, DNA-rich gapmers, and ANA.

Recently, we turned our attention to the properties of 2′F-ANA (*23*, *65*). The conformation of the 2′F-ANA strands was expected to be similar to that of DNA strands since stereoelectronic effects exerted by the *β*-2′-fluorine group stabilize the "southern/eastern" sugar conformation (*58*, *59*, *65*). Furthermore, because fluorine is smaller than a hydroxyl group, we hoped that the stability of 2′F-ANA/RNA duplexes would approach that of DNA/RNA duplexes. These expectations were confirmed. Various 2′-F ara oligomers were found to form duplexes with RNA at physiological conditions whose thermal stabilities are, in fact, higher than those of the PS-DNA and DNA oligomers (*23*). We have also recently examined the conformational preferences of a 2′F-ANA/RNA duplex by CD (*23*) and NMR (*66*) spectroscopy, and the data confirm that the structure of 2′F-ANA/RNA is highly similar to that of a native DNA/RNA hybrid.

In summary, our results indicate that ANA derivatives (such as 2′F-ANA) could serve as valuable tools for studying and controlling gene expression in cells and organisms.

SUPPORTING INFORMATION AVAILABLE

Synthetic procedures for the synthesis of arabinoinosine and arabinothymidine 3′-phosphoramidite monomers. This material is available free of charge via the Internet at http://pubs.acs.org.

REFERENCES

1. Sanghvi, Y. (1998) in *Comprehensive Natural Product Chemistry* (Barton, D. H. R., Nakanishi, K., and Meth-Coth, O., Eds.) Elsevier Science, Oxford, U.K.
2. Iyer, R. P., Roland, A., Zhou, W., and Ghosh, K. (1999) *Curr. Opin. Mol. Ther. 1*, 344−358.
3. Manoharan, M. (1999) *Biochim. Biophys. Acta 1489*, 117−130.
4. Zamecnik, P. C., and Stephenson, M. L. (1978) *Proc. Natl. Acad. Sci. U.S.A. 75*, 280−284.
5. Pon, R. T., Yu, S., Guo, Z., Yang, X., and Sanghvi, Y. S. (1999) *Nucleosides Nucleotides 18*, 1237−1238.

6. Juliano, R. L., Alahari, S., Yoo, H., Kole, R., and Cho, M. (1999) *Pharm. Res. 16*, 494−502.
7. Pon, R. T., Yu, S. Y., Guo, Z. Q., and Sanghvi, Y. S. (1999) *Nucleic Acids Res. 27*, 1531−1538.
8. Walder, R. Y., and Walder, J. A. (1988) *Proc. Natl. Acad. Sci. U.S.A. 85*, 5011−5015.
9. Uhlmann, E., and Peyman, A. (1990) *Chem. Rev. 90*, 543−584.
10. Oda, Y., Iwai, S., Ohtsuka, E., Ishikawa, M., Ikehara, M., and Nakamura, H. (1993*) Nucleic Acids Res. 21*, 4690−4695.
11. Lima, W. F., and Crooke, S. T. (1997) *Biochemistry 36*, 390−398.
12. Crooke, S. T., Lemonidis, K. M., Neilson, L., Griffey, R., Lesnik, E. A., and Monia, B. P. (1995) *Biochem. J. 312*, 599−608.
13. Federoff, O., Salazar, M., and Reid, B. R. (1993) *J. Mol. Biol. 233*, 509−523.
14. Inoue, H., Hayase, Y., Iwai, S., and Ohtsuka, E. (1987) *FEBS Lett. 215*, 327−330.
15. Nakamura, H., Oda, Y., Iwai, S., Inoue, H., Ohtsuka, S., Kanaya, S., Kimura, S., Katsuda, C., Katayanagi, K., and Morikawa, K. (1991) *Proc. Natl. Acad. Sci. U.S.A. 88*, 11535−11539.
16. Daniher, A. T., Xie, J., Mathur, S., and Bashkin, J. K. (1997) *Bioorg. Med. Chem. 5*, 1037−1042.
17. Lind, K. E., Mohan, V., Manoharan, M., and Ferguson, D. M. (1998) *Nucleic Acids Res. 26*, 3694−3699.
18. Salazar, M., Fedoroff, O. Y., and Reid, B. R. (1996) *Biochemistry 35*, 8126−8135.
19. Salazar, M., Champoux, J. J., and Reid, B. R. (1993) *Biochemistry 32*, 739−744.
20. Damha, M. J., Usman, N., and Ogilvie, K. K. (1987) *Tetrahedron Lett. 28*, 1633−1636.
21. Damha, M. J., Usman, N., and Ogilvie, K. K. (1989) *Can. J. Chem. 67*, 831−839.
22. Giannaris, P. A., and Damha, M. J. (1994) *Can. J. Chem. 72*, 909−918.
23. Damha, M. J., Wilds, C. J., Noronha, A. M., Brukner, I., Borkow, G., Arion, D., and Parniak, M. A. (1998) *J. Am. Chem. Soc. 120*, 12976−12977.
24. Puglisi, J. D., and Tinoco, I., Jr. (1989) in *Methods in Enzymology* (Dahlberg, J. E., and Abelson, J. N., Eds.) Vol. 180, pp 304−325, Academic Press, San Diego.
25. Kibler-Herzog, L., Zon, G., Whittier, G., Shaikh, M., and Wilson, W. D. (1993) *Anti-Cancer Drug Des. 8*, 63.
26. Damha, M. J., Giannaris, P. A., and Zabarylo, S. V. (1990) *Nucleic Acids Res. 18*, 3813−3821.
27. Damha, M. J., and Ogilvie, K. K. (1993) in *Methods in Molecular Biology, Vol. 20, Protocols for Oligonucleotides and Analogues: Synthesis and Properties* (Agrawal, S., Ed.) pp 81−114, Humana Press, Inc., Totowa, NJ.
28. Resmini, M., and Pfleiderer, W. (1994) *Helv. Chim. Acta 77*, 429−434.
29. Markiewicz, W. T. (1979) *J. Chem. Res. 24*, 181.
30. Pon, R. T., Usman, N., Damha, M. J., and Ogilvie, K. K. (1986) *Nucleic Acids Res. 14*, 6453−6470.
31. Robins, M. J., Wilson, J. S., Sawyer, L., and James, M. N. G. (1982) *Can. J. Chem. 81*, 1911.
32. Vorbrüggen, H., and Bennua, B. (1978) *Tetrahedron Lett. 17*, 1339−1342.
33. Ogilvie, K. K. (1972) *Carbohydr. Res. 24*, 210.
34. Barszez, D., and Shugar, D. (1968) *Eur. J. Biochem. 5*, 91.
35. Lee, J. S., Woodsworth, M. L., Latimer, L. J. P., and Morgan, A. (1984) *Nucleic Acids Res. 12*, 6603.
36. Xodo, L. E., Manzini, G., Quadrifoglio, F., van der Marel, G., and van Boom, J. H. (1991) *Nucleic Acids Res. 19*, 5625.
37. Provenzale, G., and Nagyvary, J. (1970) *Biochemistry 9*, 1744.
38. Mikita, T., and Beardsley, G. P. (1994) *Biochemistry 33*, 9195−9208.
39. Wilds, C. J. (2000) Ph.D. Thesis, McGill University, Montreal.
40. Gray, D. M., Ratliff, R. L., and Vaughan, M. R. (1992) *Methods Enzymol. 211*, 389.
41. Hung, S.-H., Yu, Q., Gray, D. M., and Ratliff, R. L. (1994) *Nucleic Acids Res. 22*, 4326−4334.
42. Ratmeyer, L., Vinayak, R., Zhong, Y. Y., Zon, G., and Wilson, W. D. (1994) *Biochemistry 33*, 5298−5304.
43. Keck, J. L., Goedken, E. R., and Marqusee, S. (1998) *J. Biol. Chem. 273*, 34128−34133.
44. Wright, G. E., and Brown, N. C. (1990) *Pharmacol. Ther. 47*, 447−497.
45. Carey, R. W., Ribas-Mundo, M., and Ellison, R. R. (1976) *Cancer 36*, 1516.
46. Kufe, D. W., and Spriggs, D. R. (1985) *Semin. Oncol. 12*, 34−38.
47. Wechter, W. J. (1967) *J. Med. Chem. 10*, 762.
48. Mikita, T., and Beardsley, G. P. (1988) *Biochemistry 27*, 4698−4705.
49. Chwang, A. K., and Sundaralingam, M. (1973) *Nature 243*, 78.
50. Teng, M.-K., Liaw, Y.-C., van der Marel, J. H., and Wang, A. H.-J. (1989) *Biochemistry 28*, 4923.
51. Gao, Y.-G., van der Marel, G. A., van Boom, and Wang, S. H.-J. (1991) *Biochemistry 30*, 9922−9931.
52. Kois, P., and Watanabe, K. A. (1993) *Nucleic Acids Symp. Ser. 29*, 215.
53. Kois, P., Tocik, Z., Spassova, M., Ren, W.-Y., Rosenberg, I., Soler, J. F., and Watanabe, K. A. (1993) *Nucleosides Nucleotides 12*, 1093.
54. Noronha, A., and Damha, M. J. (1998) *Nucleic Acids Res. 26*, 2665−2671.
55. Zubin, E. M., Antsypovich, S. I., Oretskaya, T. S., Romanova, E. A., Volkov, E. M., Tashilitsky, V. N., Dolinnaya, N. G., and Shabarova, Z. A. (1998) *Nucleosides Nucleotides 17*, 425−440.
56. Aoyagi, M., Ueno, Y., Ono, A., and Matsuda, A. (1996) *Bioorg. Med. Chem. Lett. 6*, 1573−1576.
57. Buff, R., and Hunziker, J. (1998) *Bioorg. Med. Chem. Lett. 8*, 521−524.
58. Ikeda, H., Fernandez, R., Wilk, A., Barchi, J. J., Huang, X. L., and Marquez, V. E. (1998) *Nucleic Acids Res. 26*, 2237−2244.
59. Berger, I., Tereshko, V., Ikeda, H., Marquez, V. E., and Egli, M. (1998) *Nucleic Acids Res. 26*, 2473.
60. Schmit, C., Bevierre, M. O., Demesmaeker, A., and Altmann, K. H. (1994) *Bioorg. Med. Chem. Lett. 4*, 1969−1974.
61. Gotfredsen, C. H., Spielmann, H. P., Wengel, J., and Jacobsen, J. P. (1996) *Bioconjugate Chem. 7*, 680−688.
62. Venkateswarlu, D., and Ferguson, D. M. (1999) *J. Am. Chem. Soc. 121*, 5609−5610.
63. Yathindra, N., and Sundaralingam, M. (1979) *Biochim. Biophys. Acta 564*, 301−310.
64. Monia, B. P., Lesnik, E. A., Gonzalez, C., Lima, W. F., McGee, D., Guinosso, C. J., Kawasaki, A. M., Cook, P. D., and Freier, D. (1993) *J. Biol. Chem. 268*, 14514−14522.
65. Wilds, C. J., and Damha, M. J. (1999) *Bioconjugate Chem. 10*, 299−305.
66. Trempe, J.-F., Wilds, C. J., Pon, R. T., Damha, M. J., and Gehring, K. (2000) (submitted for publication).
67. Wasner, M., Arion, D., Borkow, G., Noronha, A., Uddin, A. H., Parniak, M. A., and Damha, M. J. (1998) *Biochemistry 37*, 7478−7486.

BI000280V